Effect of band structure on field emission of crystalline graphite

2008 J. Phys.: Condens. Matter 20 035204

(http://iopscience.iop.org/0953-8984/20/3/035204)

J. Phys.: Condens. Matter **20** (2008) 035204 (6pp) doi:10.1088/0953-8984/20/03/035204

Effect of band structure on field emission of crystalline graphite

V L Katkov and V A Osipov

Joint Institute for Nuclear Research, Bogoliubov Laboratory of Theoretical Physics, 141980 Dubna, Moscow region, Russia

E-mail: katkov@theor.jinr.ru and osipov@theor.jinr.ru

Received 6 September 2007, in final form 15 November 2007
Published 10 December 2007
Online at stacks.iop.org/JPhysCM/20/035204

Abstract

The field emission of crystalline *AAA* graphite is studied within a simple analytical approach taking account of the exact dispersion relation near the Fermi level. The emission current is calculated for two crystal orientations with respect to the applied electric field. It is found that the exponent of the Fowler–Nordheim equation remains the same while the preexponential factor is markedly modified. For both field directions, the linear field dependence is found in weak fields and the standard quadratic Fowler–Nordheim behavior takes place in strong fields. A strong dependence of the emission current on the interlayer distance is observed. As an illustration of the method, the known case of a single-walled carbon nanotube is considered.

1. Introduction

Different carbon-based structures are considered as promising electrode materials for field emission (FE) cathodes. In particular, the field emission properties of single-walled (SWNTs) and multi-walled (MWNTs) carbon nanotubes [1] as well as graphite films [2] are presently under intensive experimental and theoretical investigations. In experiment, many factors such as inhomogeneities at the cathode surface, surface contamination (surface adsorbates and oxides), local electric fields and barriers, the electronic structure of cathode, etc can drastically change FE results [3]. In addition, these factors vary from one experiment to another, thus markedly complicating the theoretical description. Nevertheless, the electronic characteristics of cathodes should be equally manifested in different experiments. For this reason, the effect of electronic structure on the emission features of cathodes is of definite interest. For SWNTs this problem was studied numerically in [4–6] by using an approach which can be called a method of *independent channels*.

In this paper, we present a rather simple modification of this method to study analytically the influence of the 3D band structure on the field emission current (FEC) of crystalline graphite. As an illustration, we consider the case of SWNTs where our approach allows us to reproduce the FE results obtained in [4]. As is well-known, the electronic structure near the Fermi energy of the crystalline graphite markedly depends on the weak interlayer interaction (see, e.g. [7–10]). Accordingly, the FEC in this case should be sensitive to the specific electronic structure. In order to show this, we consider the simplest possible modification of graphite (hypothetical *AAA* stacking) where the three-dimensional energy spectrum was calculated analytically in [10]. Two possible orientations of the applied electric field (along and normal to the graphite layers) are of interest to us.

2. FEC of opened carbon SWNT

The emitted current density can be written as [3, 12]

$$j^{\mathrm{out}} = \frac{2e}{h^3}\int \mathrm{d}p_x \int \mathrm{d}p_y \int f(\varepsilon)\upsilon_{\mathrm{g}} D(\varepsilon, p_x, p_y)\,\mathrm{d}p_z. \quad (1)$$

Here the field emission is directed along the z-axis, e is the electric charge, $h = 2\pi\hbar$ the Planck constant, ε the energy, p momentum, $f(\varepsilon) = [\exp(\varepsilon/kT) + 1]^{-1}$ the Fermi–Dirac distribution function, $D(\varepsilon, p_x, p_y)$ the transmission probability of an electron through a potential barrier, and $\upsilon_{\mathrm{g}} = \partial\varepsilon/\partial p_z$ the group velocity. The integrals are over the first Brillouin zone with account taken of the positivity of υ_{g}. Notice that in most cases the use of infinite limits in integrals is a good approximation. For parabolic bands $\upsilon_{\mathrm{g}} = p_z/m$, and this relation is widely used in deriving the well-known Fowler–Nordheim equation. In the case of carbon nanotubes, two important differences from the generally accepted consideration should be taken into account.

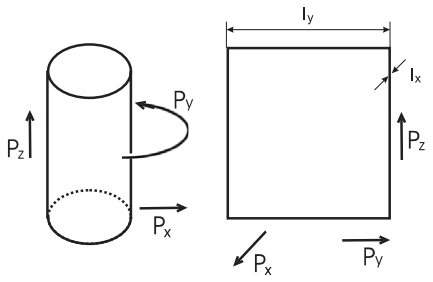

Figure 1. Selected coordinate axes for a rolled (left) and unrolled (right) nanotube. l_y is the circumference of the nanotube, l_x is a thickness of the graphite layer.

First, an open SWNT has a finite small radius which results in quantization of momentum. In this case, the corresponding integrals in (1) transform into sums. For example, choosing the axes shown in figure 1 one has $\int f(p_i)\,\mathrm{d}p_i = \sum_q f(q)h/l_i$ where $i = x, y$, l_y is the circumference of the nanotube, and l_x the thickness of the graphite layer. For a SWNT there exists only a single layer in the x-direction and, accordingly, there is exactly one term in the sum for $i = x$. The number of terms for $i = y$ depends on the tube circumference l_y.

Second, the energy near the Fermi level for a single graphite layer (graphene) is approximated by $\varepsilon = \pm\upsilon_\mathrm{F}\sqrt{p_y^2 + p_z^2}$, where υ_F is the Fermi velocity [7–10]. The electrons move in the yz plane, so that the energy does not depend on p_x. Since p_y is quantized, the energy $\varepsilon(p_y, p_z)$ turns out to be divided into a set of channels with $\varepsilon(\hbar q, p_z) = \varepsilon^q(p_z)$ where q takes integer values. Therefore, the current density (1) takes the form

$$j^\mathrm{out} = \frac{2e}{hl_x l_y}\sum_q \int f(\varepsilon^q)D(\varepsilon^q)\,\mathrm{d}\varepsilon^q. \qquad (2)$$

As is known, the dispersion relation for carbon nanotubes depends on their chirality (see, e.g. [11]). For a chiral vector (m, n) it can be written as

$$\varepsilon^q = \pm\upsilon_\mathrm{F}\left[\left(h\frac{(m-n)/3+q}{l_y}\right)^2 + p_z^2\right]^{1/2}. \qquad (3)$$

Generally, there are two symmetric curves with a gap $\varepsilon_\mathrm{g}^q = 2\upsilon_\mathrm{F}h((m-n)/3+q)/l_y$. However, at certain values of m, n, and q the gap turns out to be zero and one gets the linear dispersion relation. Therefore, at fixed q there exists one metallic branch and a set of semiconducting branches for a SWNT with a given chirality.

As stated above, the condition $\upsilon_\mathrm{g} > 0$ imposes restrictions on the limits of the integral in equation (2). In addition, two approximations will be used. First, we consider the zero-temperature limit when the Fermi–Dirac distribution becomes the step function. Second, we suggest that the transmission probability is given by the WKB approximation (see, e.g. [12, 13]) in the form

$$D(\varepsilon) = \exp\left\{-\frac{\zeta}{F}[\phi^{3/2}\upsilon(y) - 3/2\phi^{1/2}\varepsilon t(y)]\right\} = b\exp(d\varepsilon) \qquad (4)$$

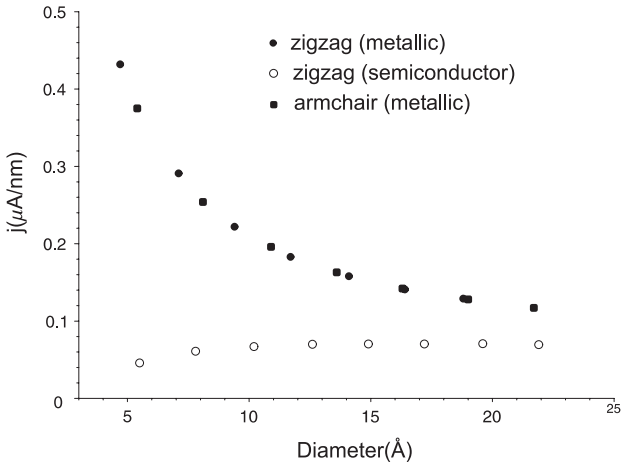

Figure 2. Current densities versus the diameter of CNTs at the applied field $F = 8\times10^9$ V m^{-1}. The parameter set is $\phi = 4.7$ eV, $\upsilon_\mathrm{F} = 0.83\times10^6$ m s^{-1}, $a = 2.46$ Å, $\zeta = 6.83\times10^9$ eV$^{-1/2}$ m^{-1}.

where $\zeta = 8\pi(2m_0)^{1/2}/3eh$, $y = (eF/4\pi\varepsilon_0)^{1/2}/\phi$, F is the electric field, ϕ the work function, ε_0 the dielectric constant, and we denoted $b = \exp\left(-\zeta\phi^{3/2}\upsilon(y)/F\right)$ and $d = 3\zeta\phi^{1/2}t(y)/2F$ for convenience. The functions $\upsilon(y)$ and $t(y)$ describe a deviation of the barrier from the triangle form due to image effects and can be approximated by [14]

$$\upsilon(y) \approx 1 - y^{1.69}, \qquad t(y) \approx 1 + 0.127y^{1.69}. \qquad (5)$$

Now we are able to calculate the qth term in the sum (2). For the metallic branch, the integration in (2) spreads from $-\infty$ to 0. One obtains

$$j_0 = \frac{4}{3}\frac{e}{hl_x l_y}\frac{F}{\zeta\phi^{1/2}t(y)}\exp\left(-\frac{\zeta}{F}\phi^{3/2}\upsilon(y)\right) = \frac{2eb}{hl_x l_y d}. \qquad (6)$$

For semiconducting branches, the range of integration in equation (2) is $(-\infty, -\varepsilon_\mathrm{g}^q/2)$ and

$$j_q = j_0\exp\left(-\frac{3}{2}\frac{\zeta\phi^{1/2}t(y)}{F}\frac{\varepsilon_\mathrm{g}^q}{2}\right) = j_0\exp\left(-d\frac{\varepsilon_\mathrm{g}^q}{2}\right). \qquad (7)$$

Notice that the dispersion relation enters equation (7) only through the gap. This agrees with the well-known fact that the group velocity and the density of states are canceled in the one-dimensional case [12].

The sum over all branches in equation (2) gives the total FEC. Figure 2 shows the calculated emission current density, which is a current divided by the circumference of a nanotube. For (m, n) SWNTs the circumference is defined as $l_y = a\sqrt{m^2 + mn + n^2}$ with a being the lattice constant. In fact, the main contribution to the sum in (2) comes from the first few terms corresponding to branches close to the Fermi level. This is due to the exponential dependence of the FEC on the gap. For metallic nanotubes, the leading term is j_0, so that $j_\mathrm{met}^\mathrm{out} \sim 1/l_y$. In the case of semiconducting nanotubes, the leading contribution comes from the qth term with the smaller gap in equation (7) and, therefore, $j_\mathrm{sem}^\mathrm{out} \sim 1/[l_y\exp(1/l_y)]$. A similar behavior was found numerically in [4]. Moreover, comparing our results in figure 2 with the exact numerical calculations

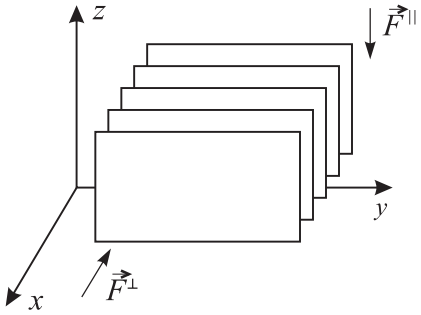

Figure 3. The location of graphite layers with respect to the electric field. The emission occurs in the direction opposite to the electric field.

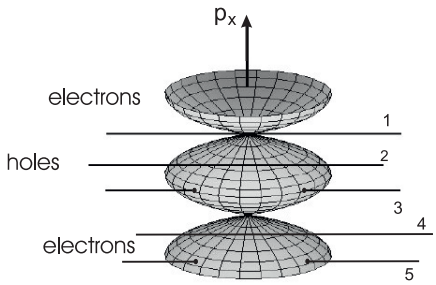

Figure 4. Fermi surface of the simple hexagonal graphite. The central pocket corresponds to the hole region, two half pockets correspond to the electron region. The solid lines show five possible types of channels for emitting electrons.

in [4] one can find out a good qualitative agreement. Notice that the quantitative difference is also not great and varies from a few to ten per cent depending on the diameter of the nanotube. In comparison with [4] our points in figure 2 are situated slightly lower for metallic nanotubes and slightly higher for semiconducting nanotubes. This difference can be explained by at least two reasons. First, we have used the simplified expression for the tunneling probability in (4) where the image effects were approximated in a standard way (see, e.g. [12, 13]). Second, as distinct from [4] we consider the zero-temperature limit.

3. FEC of crystalline graphite

3.1. Noninteracting layers

In this section, we study the case of noninteracting graphite layers. The layers are oriented as shown in figure 3. To calculate the FEC we will use the method of independent channels described in the previous section. Namely, let us consider the 2D graphite lattice with the Born–von Karman boundary conditions applied in the y-direction. This gives the natural quantization conditions. For layers of a large (infinite) size the sum in (2) can be replaced by the integral $\sum_q j_q = (l_y/h)\int j(p_y)\,\mathrm{d}p_y$, so that finally one obtains

$$j = \frac{8}{9}\frac{q}{h^2 l_x}\frac{F^2}{\zeta^2\phi\upsilon_{\mathrm{F}}t^2(y)}\exp\left(-\frac{\zeta}{F}\phi^{3/2}\upsilon(y)\right), \qquad (8)$$

where the relation $\varepsilon_{\mathrm{g}}(p_y) = 2\upsilon_{\mathrm{F}}|p_y|$ is taken into account. It is interesting to mention that this result is very similar to the Fowler–Nordheim formula

$$j^{\mathrm{FN}} = \frac{16}{9}\frac{qm_0\pi}{h^3}\frac{F^2}{\zeta^2\phi t^2(y)}\exp\left(-\frac{\zeta}{F}\phi^{3/2}\upsilon(y)\right). \qquad (9)$$

Indeed, the exponents are exactly the same and the preexponential factors differ only slightly. What is important is that the F^2-dependence is equal in both cases. For the interlayer distance $l_x = 3.34$ Å one can estimate $j/j^{\mathrm{FN}} = h/(2\upsilon_{\mathrm{F}}\pi m_0 l_x) \sim 0.4$.

3.2. AAA stacking

Generally, three possible configurations of crystalline graphite are known: $ABAB\ldots$ stacking sequence of hexagonal layers (Bernal structure), rhombohedral $ABCABC\ldots$ stacking, and $AAA\ldots$ stacking when layers of carbon atoms are located directly on top of each other [10]. The AAA stacking is called hypothetical because it has not been observed yet in crystalline graphite. However, this configuration is expected in disordered or pregraphitic carbon [16]. In this paper, we consider the model of AAA stacking which is the simplest one and allows us to study the effect of interlayer interaction on the emission properties analytically.

Let us consider the interacting graphite layers oriented parallel to the electric field (see figure 3). In the framework of the AAA model, the interaction modifies the 3D band structure near the Fermi level which can be written in a simple analytical form [10]

$$\varepsilon = 2\alpha_1\cos\left(\frac{cp_x}{\hbar}\right) \pm \alpha_0\frac{\sqrt{3}a}{2\hbar}\sqrt{p_y^2 + p_z^2}. \qquad (10)$$

Here the α_0 parameter represents the interaction between first-neighboring atoms in a layer, α_1 is related to the interaction between two atoms of the same projection on the yz plane, from two neighboring layers, and c is the interlayer spacing. The influence of other parameters α_2 and α_3 introduced in [10] is suggested to be negligible and only linear terms in the $\boldsymbol{k}\cdot\boldsymbol{p}$ perturbation expansion are taken into account. Actually, the analysis in [10] shows that the maximum effect of the next-to-leading term (breaking the cylindrical symmetry) is of the order of five per cent. The upper sign in (10) corresponds to the conduction band, and the lower sign corresponds to the valence band, $\alpha_0\sqrt{3}a/2\hbar = \upsilon_{\mathrm{F}}$.

In compliance with (10), figure 4 represents the Fermi surface of the AAA graphite. The Fermi surface is composed of a hole pocket (the valence band, 'minus' sign in (10)) and two half pockets of electrons ('plus' sign in (10)). In our case, the emission occurs along the z-axis. Generally, the possible values of the momentum of emitting electrons with respect to the Fermi surface can be collected into five different groups. We call them *independent channels*. Solid lines in figure 4 indicate five possible types of independent channels: (1) for an intermediate electron–hole region, (2, 3) for holes, and (4, 5) for electrons. For finite-size layers, quantization of momentum in the xy plane occurs. In this case, the spectrum is written as

$$\varepsilon^{ij} = 2\alpha_1\cos(cp_x^i/\hbar) \pm \upsilon_{\mathrm{F}}\sqrt{(p_y^j)^2 + p_z^2}, \qquad (11)$$

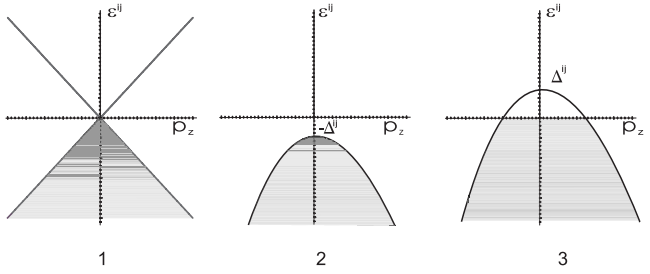

Figure 5. One-dimensional dispersion relations for the hole region.

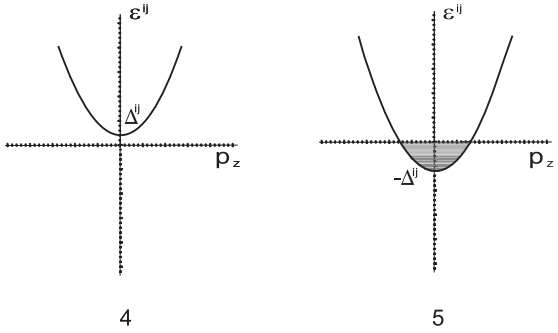

Figure 6. One-dimensional dispersion relations for the electron region.

where i, j are integers, and p_x^i lies in the region $(-\pi\hbar/c, \pi\hbar/c)$. The total FEC is a sum of all channels. Let us consider these contributions separately.

3.2.1. Hole region. The hole region is defined as $-\pi\hbar/2c < p_x^i < \pi\hbar/2c$. As is shown in figure 4 there are two types of channels for the hole region and channel 1 can be considered as an intermediate case. Figure 5 shows all possible one-dimensional dispersion relations for this case. Channel 3 crosses the Fermi surface at two points while channel 2 does not cross the Fermi surface. For each channel $j^{ij} = (2e/hl_xl_y)\int f(\varepsilon^{ij})D(\varepsilon^{ij})\,\mathrm{d}\varepsilon^{ij}$. The integration here is over the occupied states, and Δ^{ij} is the distance from the Fermi level to the extremum point of the branch (see figure 5). For channel 1 $\Delta^{ij} = 0$, and the current density is found to be equal to j_0. Notice that there are only two channels of this type. Analytically, channel 2 is defined as $|p_y^j| > \eta^i$, where $\eta^i = 2\alpha_1\cos(cp_x^i/\hbar)/\upsilon_\mathrm{F}$. For this channel one obtains

$$j^{ij} = j_0\exp(-d\Delta^{ij}). \tag{12}$$

Here Δ^{ij} takes the form $\Delta^{ij} = \upsilon_\mathrm{F}|p_y^j| - 2\alpha_1\cos(cp_x^i/\hbar)$, which can be easily found from (11). Replacing the sum $\sum_{ij} j^{ij}$ by the integral one gets

$$j_2^\parallel = \frac{2l_xl_y}{h^2}\int_{-h/4c}^{h/4c}\mathrm{d}p_x\int_\eta^\infty j_0\exp[-d\Delta(p_x, p_y)]\,\mathrm{d}p_y = \frac{2eb}{h^2d^2c\upsilon_\mathrm{F}}. \tag{13}$$

For channel 3 one has $|p_y^j| < \eta^i$ and $j^{ij} = j_0$. As before, one obtains

$$j_3^\parallel = \frac{2l_xl_y}{h^2}\int_{-h/4c}^{h/4c}\mathrm{d}p_x\int_0^\eta j_0\,\mathrm{d}p_y = \frac{8\alpha_1eb}{\pi h^2dc\upsilon_\mathrm{F}}. \tag{14}$$

3.2.2. Electron region. The electron region is defined as $-\pi\hbar/c < p_x^i < -\pi\hbar/2c$ and $\pi\hbar/2c < p_x^i < \pi\hbar/c$ or, taking into account a periodicity of the Brillouin zone, $\pi\hbar/2c < p_x^i < 3\pi\hbar/2c$. There are two kinds of channels in the electron region with spectra shown in figure 6. Channel 4 does not cross the Fermi surface and, therefore, the current density turns out to be zero. For channel 5 one has $|p_y^j| < |\eta^i|$. This channel contains occupied states below the Fermi level and, hence, there is a nonzero contribution to the FEC. One obtains

$$j^{ij} = j_0[1 - \exp(-d\Delta^{ij})], \tag{15}$$

where $\Delta^{ij} = 2\alpha_1|\cos(cp_x^i/\hbar)| - \upsilon_\mathrm{F}|p_y^j|$ in accordance with equation (11). Finally,

$$j_5^\parallel = \frac{2l_xl_y}{h^2}\int_{h/4c}^{3h/4c}\mathrm{d}p_x\int_0^\eta j_0\{1 - \exp[-d\Delta(p_x, p_y)]\}\,\mathrm{d}p_y = \frac{2eb[4d\alpha_1/\pi + (\mathbf{I}_0(2d\alpha_1) - \mathbf{L}_0(2d\alpha_1) - 1)]}{d^2c\upsilon_\mathrm{F}h^2}, \tag{16}$$

where $\mathbf{L}_0(x)$ is the modified Struve function, and $\mathbf{I}_0(x)$ is the modified Bessel function.

3.2.3. Resulting FEC. The total current density is found to be

$$j_\mathrm{tot}^\parallel = \sum_{i=2}^{5} j_i^\parallel = \frac{2eb[8d\alpha_1/\pi + \mathbf{I}_0(2d\alpha_1) - \mathbf{L}_0(2d\alpha_1)]}{h^2d^2c\upsilon_\mathrm{F}}. \tag{17}$$

Notice that $j_\mathrm{tot}^\parallel$ reduces to (8) for $\alpha_1 = 0$.

3.3. AAA stacking: perpendicular electric field

Let us consider interacting graphite layers placed normally to the electric field (see figure 3). This situation differs markedly from the previous case. Let us denote $\rho = \sqrt{p_y^2 + p_z^2}$ in the dispersion relation in equation (10). Quantization of momentum results in the replacement $\rho \to \rho^{ij}$. There are only two types of channels in this case (see figure 7). As before, let us consider them separately.

3.3.1. Hole region. The hole region is defined by $-\pi\hbar/2c < p_x < \pi\hbar/2c$. There are two kinds of channels in the hole region with spectra shown in figure 8. Channel 1 is defined by $\rho^{ij} < 2\alpha_1/\upsilon_\mathrm{F}$. The current density reads

$$j^{ij} = j_0[1 - \exp(-d\Delta^{ij})], \tag{18}$$

where $\Delta^{ij} = \upsilon_\mathrm{F}\rho^{ij}$. One obtains

$$j_1^\perp = \frac{l_yl_z}{h^2}\int_0^{2\alpha_1/\upsilon_\mathrm{F}} j_0\{1 - \exp[-d\Delta(\rho)]\}2\pi\rho\,\mathrm{d}\rho = \frac{4\pi eb}{(dh)^3\upsilon_\mathrm{F}^2}\left(\frac{(2\alpha_1d)^2}{2} - 1 + \exp(-2\alpha_1d)(2\alpha_1d + 1)\right). \tag{19}$$

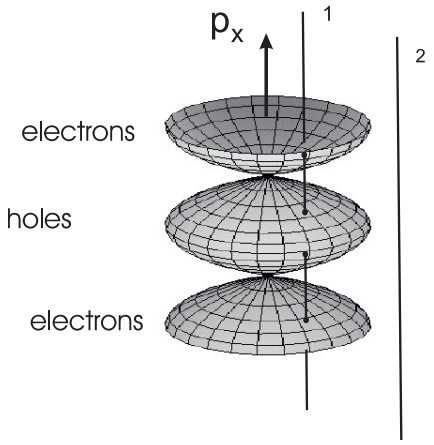

Figure 7. Fermi surface of simple hexagonal graphite. The solid lines show two possible types of channels for electrons emitted in the x-direction.

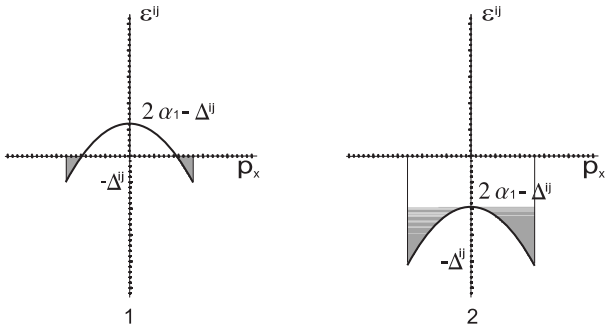

Figure 8. One-dimensional dispersion relations for the hole region.

Channel 2 is defined by $\rho^{ij} > 2\alpha_1/\upsilon_F$, and

$$j^{ij} = j_0(\exp(2\alpha_1 d) - 1)\exp(-d\Delta^{ij}). \tag{20}$$

Finally,

$$j_2^{\perp} = \frac{l_y l_z}{h^2}\int_0^{2\alpha_1/\upsilon_F} j_0(\exp(2\alpha_1 d) - 1)\exp[-d\Delta(\rho)]2\pi\rho\,\mathrm{d}\rho$$
$$= \frac{4\pi eb(2\alpha_1 d + 1)}{(dh)^3\upsilon_F^2}\exp(-2\alpha_1 d)(\exp(2\alpha_1 d) - 1). \tag{21}$$

3.3.2. Electron region. In the electron region $\pi\hbar/2c < p_x < 3\pi\hbar/2c$. There are also two kinds of channels in this region with spectra shown in figure 9. Channel 3 is equivalent to channel 5 in the previous section. It is defined by $\rho^{ij} < 2\alpha_1/\upsilon_F$. The current is

$$j^{ij} = j_0[1 - \exp(-d\Delta^{ij})]. \tag{22}$$

Here $\Delta^{ij} = 2\alpha_1 - \upsilon_F\rho^{ij}$ (see figure 9 and equation (11)). In this case,

$$j_4^{\perp} = \frac{l_y l_z}{h^2}\int_0^{2\alpha_1/\upsilon_F} j_0\{1 - \exp[-d\Delta(\rho)]\}2\pi\rho\,\mathrm{d}\rho$$
$$= \frac{4\pi eb}{(dh)^3\upsilon_F^2}\left(\frac{(2\alpha_1 d)^2}{2} - 2\alpha_1 d + \exp(2\alpha_1 d) - 1\right). \tag{23}$$

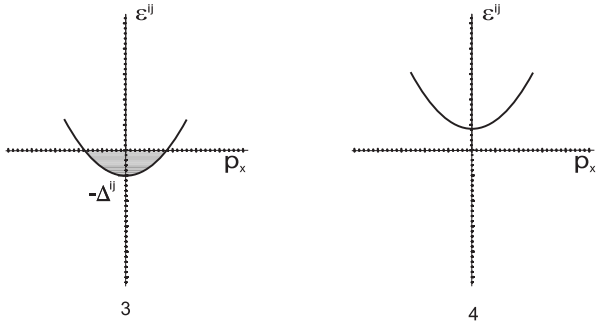

Figure 9. One-dimensional dispersion relations for the electron region.

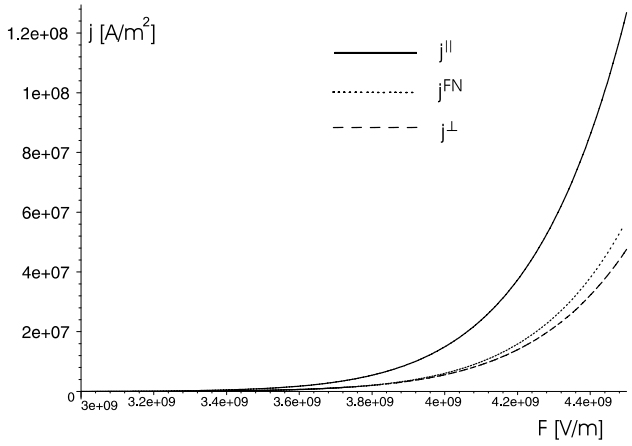

Figure 10. The current densities versus electric field for graphite layers placed parallel ($j^{\parallel}$) and normal ($j^{\perp}$) to the electric field with $\alpha_1 = 0.4$ eV, $\phi = 5$ eV. For comparison the Fowler–Nordheim curve (j^{FN}) is shown.

Channel 4 is defined by $\rho^{ij} > 2\alpha_1/\upsilon_F$. Since it does not cross the Fermi surface the current density is equal to zero.

3.3.3. Resulting FEC. The total current density is the sum of all channels

$$j_{\mathrm{tot}}^{\perp} = \frac{4\pi eb}{(dh)^3\upsilon_F^2}\left[(2\alpha_1 d)^2 + 1 - \exp(-2\alpha_1 d)\right]. \tag{24}$$

4. Discussion

Figure 10 shows the calculated current densities as functions of the applied electric field. For comparison, the Fowler–Nordheim curve is drawn. The most important difference comes from preexponential factors. As is known, the Fowler–Nordheim theory gives $j^{\mathrm{FN}} \sim F^2 b$ at all F. In accordance with equation (17) the preexponential factor has a different field dependence. At small F one obtains $j^{\parallel} \sim Fb$. When F increases (which means $2\alpha_1 d \to 0$) the current density comes to $j^{\parallel} \sim F^2 b$ and, finally, $j^{\parallel}/j^{\mathrm{FN}} \to 0.4$ as was shown in section 3.1. Indeed, at large x the difference $\mathbf{I}_0(x) - \mathbf{L}_0(x)$ tends to $2/(\pi x)$ while at small x it tends to 1 [15]. This is clearly seen in figure 11 where the comparative curves are demonstrated. For $j^{\perp}$ we have a similar behavior. According

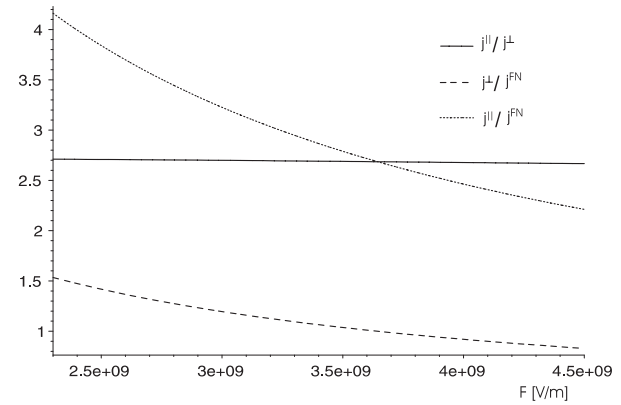

Figure 11. Comparative curves for the current densities versus the electric field characterizing the role of the preexponential factor. $j^{\parallel}/j^{\perp}$ is almost a constant in the considered interval of F.

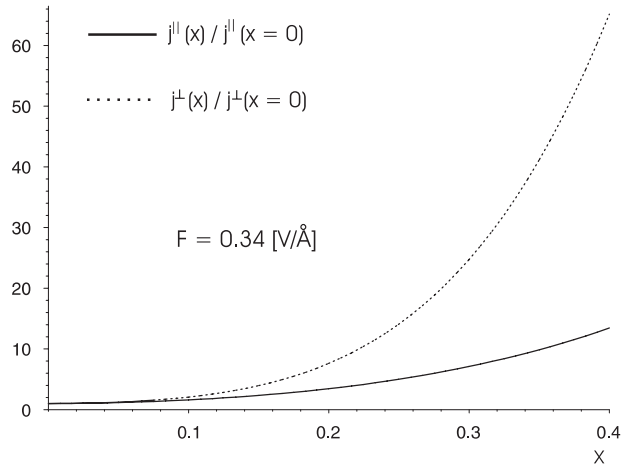

Figure 12. Reduced current density versus relative interlayer distance $x = (c - c^*)/c$, $c = 3.34$ Å for two field orientations. $j^{\perp}$ is markedly more sensitive to x than $j^{\parallel}$.

to equation (24), $j^{\perp} \sim \alpha_1^2 F b$ at small F and $j^{\perp} \sim \alpha_1 F^2 b$ at large F, so that $j^{\perp}/j^{\mathrm{FN}}$ tends to a constant with increasing F. One can conclude that the bigger the electric field the lesser is the role of the interlayer interaction. The anisotropy of the emission from the 3D graphite is also shown in figure 11. As is seen, $j^{\parallel}/j^{\perp} \sim 2.7$, which is almost a constant in the considered interval of F. Therefore, we obtain a three times increase in FEC when graphite layers are oriented in parallel with the electric field.

It is interesting to discuss the dependence of FEC from the parameter α_1 which characterizes the interlayer interaction. It was found in [16] that this parameter is very sensitive to the interlayer distance. Based on their results one can approximate

$$\alpha_1 = 18x^2 - 0.4, \tag{25}$$

where $x = (c - c^*)/c$ and α_1 is measured in eV. As is seen from figure 12, there is a strong dependence of the FEC on the interlayer distance. The less is this distance the more is the emission current. This is valid for both orientations. It would be interesting to check this finding in experiments with graphite crystals under pressure. Notice that this result follows from the fact that the DOS at the Fermi level (which is of most importance in the emission process) is determined by α_1 (see [10]). As is seen from figure 12, $j^{\perp}$ is more sensitive to x than $j^{\parallel}$. Moreover, for $\alpha_1 \to 0$ one has $j^{\perp} \to 0$, which follows from the fact that the movement of electrons between layers is suppressed in the absence of the interlayer interaction.

5. Conclusion

In conclusion, we have found that the band structure of the 3D graphite has a marked impact on the field emission current. Experimentally, the field emission from carbon materials was studied in [2]. Unfortunately, the polycrystalline carbon films used in experiment cannot be properly described in the framework of our approach because for this purpose we have to consider a mixture between different crystalline structures. In fact, the Fermi surface of the $ABAB$ structure of graphite is found to be much more complex and, in particular, it does not possess cylindrical symmetry (see, e.g. [9, 16]). In this case, our approach should be markedly modified. Besides, many additional factors such as the presence of a diamond-like phase on the surface of samples and the absence of any information about the local electric fields do not allow us to clarify the role of the band structure in this case. Therefore, specific emission experiments with graphite single crystals at different orientations of the electric field would be of evident interest.

Acknowledgment

This work has been supported by the Russian Foundation for Basic Research under grant no. 05-02-17721.

References

[1] Jonge B N and Bonard J 2004 *Phil. Trans. R. Soc.* A **362** 2239
[2] Obraztsov A N, Volkov A P and Pavlovskii I Yu 1998 *JETP Lett.* **68** 59
[3] Modinos A 1984 *Field-, Thermionic- and Secondary Electron Emission Spectroscopy* (New York: Plenum)
[4] Shi-Dong L and Xu N S 2003 *Appl. Phys. Lett.* **83** 1213
[5] Shi-Dong L, Huang N Y, Deng S Z and Xu N S 2004 *Appl. Phys. Lett.* **85** 813
[6] Xinghui L, Changchun Z and Yukui L 2003 *Physica* B **344** 243
[7] Wallace P R 1947 *Phys. Rev.* **71** 622
[8] Slonczewski J C 1958 *Phys. Rev.* **109** 272
[9] McClure J W 1964 *IBM J. Res. Dev.* **8** 255
[10] Charlier J C, Michenaud J P, Gonze X and Vigneron J P 1991 *Phys. Rev.* B **44** 13237
[11] Saito R, Fujita M, Dresselhaus G and Dresselhaus M S 1992 *Appl. Phys. Lett.* **60** 2204
[12] Gadzuk J W and Plummer E W 1973 *Rev. Mod. Phys.* **45** 487
[13] Edgcombe C J 2002 *Phil. Mag.* B **82** 1009
[14] Hawkes P W and Kasper E 1989 *Principles of Electron Optic* vol 2 (London: Academic)
[15] Abramowitz M and Stegun I 1984 *Handbook of Mathematical Function* vol 12.2.6. (New York: Dover)
[16] Charlier J C, Michenaud J P and Gonze X 1992 *Phys. Rev.* B **46** 4531